12

Magnetoelectric Multiferroic Composites

M. I. Bichurin[1], V. M. Petrov[1] and S.Priya[2]
[1]*Novgorod State University*
[2]*Virginia Tech*
[1]*Russia*
[2]*USA*

1. Introduction

Magnetoelectric (ME) multiferroics are materials in which ferromagnetism and ferroelectricity occur simultaneously and coupling between the two is enabled. Applied magnetic field $\boldsymbol{H}$ gives rise to an induced polarization $\boldsymbol{P}$ which can be expressed in terms of magnetic field by the expression, $\boldsymbol{P}=\boldsymbol{\alpha}\boldsymbol{H}$, where $\boldsymbol{\alpha}$ is the ME-susceptibility tensor. Most of the known single-phase ME materials are known to show a weak ME coupling (Fiebig, 2005; Kita et al., 1988; Wang et al., 2003; Prellier et al., 2005; Cheong et al., 2007). A composite of piezomagnetic and piezoelectric phases is expected to have relatively strong ME coupling. ME interaction in a composite manifests itself as inducing the electrical voltage across the sample in an applied ac magnetic field and arises due to combination of magnetostriction in magnetic phase and piezoelectricity in piezoelectric phase through mechanical coupling between the components (Ryu et al., 2001; Nan et al., 2008; Dong et al., 2003; Cai et al., 2004; Srinivasan et al., 2002).

In last few years, strong magneto-elastic and elasto-electric coupling has been achieved through optimization of material properties and proper design of transducer structures. Lead zirconate titanate (PZT)-ferrite and PZT-Terfenol-D are the most studied composites to-date (Dong et al., 2005; Dong et al.,2006b; Zheng et al., 2004a; Zheng et al., 2004b). One of largest ME voltage coefficient of 500 $Vcm^{-1}Oe^{-1}$ was reported recently for a high permeability magnetostrictive piezofiber laminate (Nan et al., 2005; Liu et al., 2005). These developments have led to magnetoelectric structures that provide high sensitivity over a varying range of frequency and DC bias fields enabling the possibility of practical applications.

In this paper, we focus on four broad objectives. First, we discuss detailed mathematical modeling approaches that are used to describe the dynamic behavior of ME coupling in magnetostrictive-piezoelectric multiferroics at low-frequencies and in electromechanical resonance (EMR) region. Expressions for ME coefficients were obtained using the solution of elastostatic/elastodynamic and electrostatic/magnetostatic equations. The ME voltage coefficients were estimated from the known material parameters. The basic methods developed for decreasing the resonance frequencies were analyzed. The second type of resonance phenomena occurs in the magnetic phase of the magnetoelectric composite at much higher frequencies, called as ferromagnetic resonance (FMR). The estimates for electric field induced shift of magnetic resonance line were derived and analyzed for

varying boundary conditions. Our theory predicts an enhancement of ME effect that arises from interaction between elastic modes and the uniform precession spin-wave mode. The peak ME voltage coefficient occurs at the merging point of acoustic resonance and FMR frequencies.

Second, we present the experimental results on lead – free magnetostrictive –piezoelectric composites. These newly developed composites address the important environmental concern of current times, i.e., elimination of the toxic "lead" from the consumer devices. A systematic study is presented towards selection and design of the individual phases for the composite. Third, experimental data from wide range of measurement and literature was used to validate the theoretical models over a wide frequency range.

Lastly, the feasibility for creating new class of functional devices based on ME interactions is addressed. Appropriate choice of individual phases with high magnetostriction and piezoelectricity will allow reaching the desired magnitude of ME coupling as deemed necessary for engineering applications over a wide bandwidth including the electromechanical, magnetoacoustic and ferromagnetic resonance regimes. Possibilities for application of ME composites in fabricating ac magnetic field sensors, current sensors, transformers, and gyrators are discussed. ME multiferroics are shown to be of interest for applications such as electrically-tunable microwave phase-shifters, devices based on FMR, magnetic-controlled electro-optical and piezoelectric devices, and electrically-readable magnetic memories.

2. Low-frequency magnetoelectric effect in magnetostrictive-piezoelectric bilayers

We consider only (symmetric) extensional deformation in this model and at first ignore any (asymmetric) flexural deformations of the layers that would lead to a position dependent elastic constants and the need for perturbation procedures. For the polarized piezoelectric phase with the symmetry ∞m, the following equations can be written for the strain and electric displacement:

$$\begin{aligned} {}^{p}S_i &= {}^{p}s_{ij}\,{}^{p}T_j + {}^{p}d_{ki}\,{}^{p}E_k; \\ {}^{p}D_k &= {}^{p}d_{ki}\,{}^{p}T_i + {}^{p}\varepsilon_{kn}\,{}^{p}E_n; \end{aligned} \tag{1}$$

where ${}^{p}S_i$ and ${}^{p}T_j$ are strain and stress tensor components of the piezoelectric phase, ${}^{p}E_k$ and ${}^{p}D_k$ are the vector components of electric field and electric displacement, ${}^{p}s_{ij}$ and ${}^{p}d_{ki}$ are compliance and piezoelectric coefficients, and ${}^{p}\varepsilon_{kn}$ is the permittivity matrix. The magnetostrictive phase is assumed to have a cubic symmetry and is described by the equations:

$$\begin{aligned} {}^{m}S_i &= {}^{m}s_{ij}\,{}^{m}T_j + {}^{m}q_{ki}\,{}^{m}H_k; \\ {}^{m}B_k &= {}^{m}q_{ki}\,{}^{m}T_i + {}^{m}\mu_{kn}\,{}^{m}H_n; \end{aligned} \tag{2}$$

where ${}^{m}S_i$ and ${}^{m}T_j$ are strain and stress tensor components of the magnetostrictive phase, ${}^{m}H_k$ and ${}^{m}B_k$ are the vector components of magnetic field and magnetic induction, ${}^{m}s_{ij}$ and ${}^{m}q_{ki}$ are compliance and piezomagnetic coefficients, and ${}^{m}\mu_{kn}$ is the permeability matrix. Equation (2) may be considered in particular as a linearized equation describing the effect of

magnetostriction. Assuming in-plane mechanical connectivity between the two phases with appropriate boundary conditions, ME voltage coefficients can be obtained by solving Eqs.(1) and (2).

2.1 Longitudinal ME effect

We assume (*1,2*) as the film plane and the direction-*3* perpendicular to the sample plane. The bilayer is poled with an electric field *E* along direction-*3*. The bias field H_0 and the ac field *H* are along the same direction as *E* and the resulting induced electric field *E* is estimated across the sample thickness. Then we find an expression for ME voltage coefficient $a_{E,L}=a_{E,33}=E_3/H_3$. The following boundary conditions should be used for finding the ME coefficient:

$$\begin{aligned} {}^{p}S_i &= {}^{m}S_i;\ (i=1,2)\ ; \\ {}^{p}T_i &= -{}^{m}T_i(1-v)/\ v;(i=1,2); \end{aligned} \tag{3}$$

where $v={}^{p}v/({}^{p}v+{}^{m}v)$ and ${}^{p}v$ and ${}^{m}v$ denote the volume of piezoelectric and magnetostrictive phase, respectively. Taking into account Eqs. (1) and (2) and the continuity conditions for magnetic and electric fields, Eqs. (3) and open circuit condition enables one to obtain the following expressions for longitudinal ME voltage coefficient.

$$\alpha_{E,33}=\frac{E_3}{H_3}=2\frac{\mu_0 v(1-v)\,{}^{p}d_{31}\,{}^{m}q_{31}}{\{2\,{}^{p}d_{31}^2(1-v)+{}^{p}\varepsilon_{33}[({}^{p}s_{11}+{}^{p}s_{12})(v-1)-v({}^{m}s_{11}+{}^{m}s_{12})]\}}\times \\ \times\frac{[({}^{p}s_{11}+{}^{p}s_{12})(v-1)-v({}^{m}s_{11}+{}^{m}s_{12})]}{\{[\mu_0(v-1)-{}^{m}\mu_{33}v][v({}^{m}s_{12}+{}^{m}s_{11})-({}^{p}s_{11}+{}^{p}s_{12})(v-1)]+2\,{}^{m}q_{31}^2v^2\}} \tag{4}$$

In deriving the above expression, we assumed the electric field to be zero in magnetic phase since magnetostrictive materials that are used in the case under study have a small resistance compared to piezoelectric phase. Thus the voltage induced across the piezoelectric layer is the output voltage. Estimate of ME voltage coefficient for cobalt ferrite (CFO) gives $\alpha_{E,33}$=325 mV/(cm Oe). However, considering CFO as a dielectric results in $\alpha_{E,33}$=140 mV/(cm Oe) (Osaretin & Rojas, 2010) while the experimental value is 74 mV/(cm Oe) (Harshe et al., 1993). We believe CFO should be considered as a conducting medium compared to dielectric PZT in the low-frequency region in accordance with our model. The discrepancy between theoretical estimates and data can be accounted for by features of piezomagnetic coupling in CFO and interface coupling of bilayer (Bichurin et al., 2003a). Harshe et al. obtained an expression for longitudinal ME voltage coefficient of the form

$$\alpha'_{E,33}=\frac{-2v(v-1)^{p}d_{13}\,{}^{m}q_{31}}{\left({}^{m}s_{11}+{}^{m}s_{12}\right)^{p}\varepsilon^{T}{}_{33}v\ +\ \left({}^{p}s_{11}+{}^{p}s_{12}\right)^{p}\varepsilon^{T}{}_{33}(1-v)\ -2\left({}^{p}d_{13}\right)^2(1-v)} \tag{5}$$

The above equation corresponds to a special case of our theory in which one assumes ${}^{m}\mu_{33}/\mu_0=1$. Thus the model considered here leads to an expression for the longitudinal ME coupling and allows its estimation as a function of volume of the two phases, composite permeability, and interface coupling.

2.2 Transverse ME effect

This case corresponds to the poling direction along direction-*3* and H_0 and H along direction-*1* (in the sample plane). Here we estimate the ME coefficient $a_{E,T} = a_{E,31} = E_3/H_1$. Once again, Eqs.(1)-(3) lead to the following expression for transverse ME voltage coefficient.

$$\alpha_{E,31} = \frac{E_3}{H_1} = \frac{-v(1-v)({}^{m}q_{11} + {}^{m}q_{21})\,{}^{p}d_{31}}{{}^{p}\varepsilon_{33}({}^{m}s_{12} + {}^{m}s_{11})v + {}^{p}\varepsilon_{33}({}^{p}s_{11} + {}^{p}s_{12})(1-v) - 2\,{}^{p}d_{31}^{2}(1-v)} \tag{6}$$

2.3 In-plane longitudinal ME effect

Finally, we consider a bilayer poled with an electric field E in the plane of the sample. The in-plane fields H_0 and H are parallel and the induced electric field E is measured in the same direction (axis-*1*). The ME coefficient is defined as $a_{E,IL}=a_{E,11}=E_1/H_1$. Expression for a_E is given below.

$$\begin{aligned}
\alpha_{E,11} = {} & \left(\left({}^{m}q_{11}\left({}^{p}s_{33}\,{}^{p}d_{11} - {}^{p}s_{12}\,{}^{p}d_{12}\right) + {}^{m}q_{12}\left({}^{p}s_{11}\,{}^{p}d_{12} - {}^{p}s_{12}\,{}^{p}d_{11}\right)\right)(1-v) + \right. \\
& \left. + \left({}^{m}q_{11}\left({}^{m}s_{11}\,{}^{p}d_{11} - {}^{m}s_{12}\,{}^{p}d_{12}\right) + {}^{m}q_{12}\left({}^{m}s_{11}\,{}^{p}d_{12} - {}^{m}s_{12}\,{}^{p}d_{11}\right)\right)v\right)v(1-v) \Big/ \\
& \Big/ \left(\left((1-p)\,{}^{m}\varepsilon_{11} + v\,{}^{p}\varepsilon_{11}\right)\left[(1-v)^{2}\left({}^{p}s_{11}\,{}^{p}s_{33} - {}^{p}s_{12}^{2}\right) + (1-v)v({}^{m}s_{11}\,{}^{p}s_{11} + {}^{p}s_{33}\,{}^{m}s_{11} - \right.\right. \\
& \left.\left. - 2\,{}^{p}s_{12}\,{}^{m}s_{12}\right] + v^{2}\left({}^{m}s_{11}^{2} - {}^{m}s_{12}^{2}\right)\right) - v(1-p)^{2}\left[2\,{}^{p}s_{12}\,{}^{p}d_{11}\,{}^{p}d_{12} - {}^{p}s_{33}\,{}^{p}d_{11}^{2} - \right. \\
& \left. - {}^{p}s_{11}\,{}^{p}d_{12}^{2}\right] + v^{2}(1-v)\left({}^{m}s_{11}\,{}^{p}d_{12}^{2} + {}^{m}s_{11}\,{}^{p}d_{11}^{2} - 2\,{}^{m}s_{12}\,{}^{p}d_{12}\,{}^{p}d_{11}\right)\Big)
\end{aligned} \tag{7}$$

The in-plane ME coefficient is expected to be the strongest amongst the cases discussed so far due to high values of q and d and the absences of demagnetizing fields.

3. ME effect at longitudinal modes of EMR

Since the ME coupling in the composites is mediated by the mechanical stress, one would expect orders of magnitude stronger coupling when the frequency of the ac field is tuned to acoustic mode frequencies in the sample than at non-resonance frequencies. Two methods of theoretical modeling can be used for calculating the frequency dependence of ME coefficients by solving the medium motion equation. First approach rests on considering the structure as an effective homogeneous medium and implies the preliminary finding the effective low-frequency material parameters (Bichurin et al., 2003b). The second approach is based on using the initial material parameters of components. A recently reported attempt to estimate ME coefficients using this approach consists in supposing the magnetic layer to move freely, ignoring the bonding to piezoelectric layer while vibration of piezoelectric layer is supposed to be a combination of motions of free magnetic layer and free oscillations of piezoelectric layer (Filippov, 2004, 2005). In case of perfect bonding of layers, the motion of piezoelectric phase is described by magnetic medium motion equation. As a result, the expressions for ME coefficients appear inaccurate. Particularly, the expressions give a wrong piezoelectric volume fraction dependence of ME voltage coefficient.

This section is focused on modeling of the ME effect in ferrite-piezoelectric layered structures in EMR region. We have chosen cobalt ferrite (CFO) - barium titanate as the

model system for numerical estimations. The ME voltage coefficients a_E have been estimated for transverse field orientations corresponding to minimum demagnetizing fields and maximum a_E. (Bichurin et al., 2010) As a model, we consider a ferrite-piezoelectric layered structure in the form of a thin plate with the length L.

We solve the equation of medium motion taking into account the magnetostatic and elastostatic equations, constitutive equations, Hooke's law, and boundary conditions. The equation of medium motion has the form:

$$\frac{\partial^2 u_1}{\partial x^2} = -k^2 u_1 ; \tag{8}$$

where u_1 is displacement in the traveling direction x. For the transverse fields' orientation (poling direction of piezoelectric phase, dc and ac magnetic fields are parallel to x-axis), the wave value k is defined by expression:

$$k = \omega \sqrt{\left[{}^{p}\rho\, v + {}^{m}\rho(1-v) \right] \left[\frac{v}{{}^{p}s_{11}} + \frac{1-v}{{}^{m}s_{11}} \right]^{-1}} ; \tag{9}$$

where ω is the circular frequency, ${}^{p}\rho$ and ${}^{m}\rho$ are the piezoelectric and piezomagnetic densities, $v = {}^{p}v/({}^{p}v + {}^{m}v)$, and ${}^{p}v$ and ${}^{m}v$ denote the volume of piezoelectric and phases, respectively. For the solution of the Eq. (8), the following boundary conditions are used: ${}^{p}S_1 = {}^{m}S_1$ and ${}^{p}T_1 v + {}^{m}T_1 (1-v) = 0$ at x=0 and x=L, where L is the sample length. The ME voltage coefficient $a_{E\,13} = E_3/H_1$ is calculated from Eqs. (8), (9) and using the open circuit condition $D_3 = 0$.

$$\alpha_{E,31} = \frac{2\,{}^{p}d_{31}\,{}^{m}g_{11}\mu_{eff}\,{}^{p}s_{11} v(1-v)\tan(kL/2)}{s_2({}^{p}d_{31}^2 - {}^{p}s_{11}\,{}^{p}\varepsilon_{33})kL - 2\,{}^{p}d_{31}^2 v\,{}^{m}s_{11}^{B}\tan(kL/2)} ; \tag{10}$$

where $s_2 = v\,{}^{m}s^{B}_{11} + (1-v)\,{}^{p}s_{11}$ and μ_{eff} is effective permeability of piezomagnetic layer. To take into consideration the energy loss, we set ω equal to $\omega' - i\omega''$ with $\omega''/\omega' = 10^{-3}$. The resonance enhancement of ME voltage coefficient for the bilayer is obtained at antiresonance frequency. ME voltage coefficient, $a_{E,13}$ increases with increasing barium titanate volume, attains a peak value for v = 0.5 and then drops with increasing v as in Fig. 1.

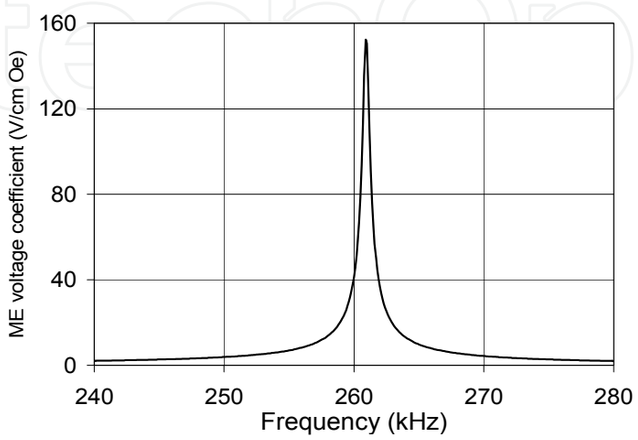

Fig. 1. Frequency dependence of $a_{E,13}$ for the bilayer with v=0.5

4. ME effect at bending modes of EMR

A key drawback for ME effect at longitudinal modes is that the frequencies are quite high, on the order of hundreds of kHz, for nominal sample dimensions. The eddy current losses for the magnetostrictive phase can be quite high at such frequencies, in particular for transition metals and alloys and earth rare alloys such as Terfenol-D, resulting in an inefficient magnetoelectric energy conversion. In order to reduce the operating frequency, one must therefore increase the laminate size that is inconvenient for any applications. An alternative for getting a strong ME coupling is the resonance enhancement at bending modes of the composite. The frequency of applied ac field is expected to be much lower compared to longitudinal acoustic modes. Recent investigations have showed a giant ME effect at bending modes in several layered structures (Xing et al., 2006; Zhai et al., 2008; Chashin et al., 2008). In this section, we focus our attention on theoretical modeling of ME effects at bending modes. (Petrov et al., 2009)

An in-plane bias field is assumed to be applied to magnetostrictive component to avoid the demagnetizing field. The thickness of the plate is assumed to be small compared to remaining dimensions. Moreover, the plate width is assumed small compared to its length. In that case, we can consider only one component of strain and stress tensors in the EMR region. The equation of bending motion of bilayer has the form:

$$\nabla^2\nabla^2 w + \frac{\rho\, b}{D}\frac{\partial^2 w}{\partial \tau^2} = 0\,; \tag{11}$$

where $\nabla^2\nabla^2$ is biharmonic operator, w is the deflection (displacement in z-direction), t and ρ are thickness and average density of sample, $b = {}^{p}t + {}^{m}t$, $\rho = ({}^{p}\rho\, {}^{p}t + {}^{m}\rho\, {}^{m}t)/b$, ${}^{p}\rho$, ${}^{m}\rho$, and ${}^{p}t$, ${}^{m}t$, are densities and thicknesses of piezoelectric and piezomagnetic, correspondingly, and D is cylindrical stiffness.

The boundary conditions for $x=0$ and $x=L$ have to be used for finding the solution of above equation. Here L is length of bilayer. As an example, we consider the plate with free ends. At free end, the turning moment M_1 and transverse force V_1 equal zero: $M_1 = 0$ and $V_1 = 0$ at x=0 and x=L, where $M_1 = \int_A z T_1 dz_1$, $V_1 = \frac{\partial M_1}{\partial x}$, and A is the cross-sectional area of the sample normal to the x-axis. We are interested in the dynamic ME effect; for an ac magnetic field H applied to a biased sample, one measures the average induced electric field and calculates the ME voltage coefficient. Using the open circuit condition, the ME voltage coefficient can be found as

$$\alpha_{E\,31} = \frac{E_3}{H_1} = -\frac{\int_{z_0 - {}^{p}t}^{z_0} {}^{p}E_3 dz}{t\, H_1\, {}^{p}\varepsilon_{33}}\,; \tag{12}$$

where E_3 and H_1 are the average electric field induced across the sample and applied magnetic field. The energy losses are taken into account by substituting ω for complex frequency $\omega' + i\omega''$ with $\omega''/\omega' = 10^{-3}$.

As an example, we apply Eq. 12 to the bilayer of permendur and PZT. Fig. 2 shows the frequency dependence of ME voltage coefficient at bending mode for free-standing bilayer

with length 9.15 mm and thickness 3.22 mm for PZT volume fraction 0.67. Graph of $a_{E,31}$ reveals a giant value $a_{E\ 31}$=*6.6 V/cm Oe* and resonance peak lies in the infralow frequency range. Fig. 3 reveals the theoretical and measured frequency dependencies of transverse ME voltage coefficients for a permendur-PZT bilayer that is free to bend at both ends.
According to our model, there is a strong dependence of resonance frequency on boundary conditions. The lowest resonance frequency is expected for the bilayer clamped at one end. One expects bending motion to occur at decreasing frequencies with increasing bilayer length or decreasing thickness.

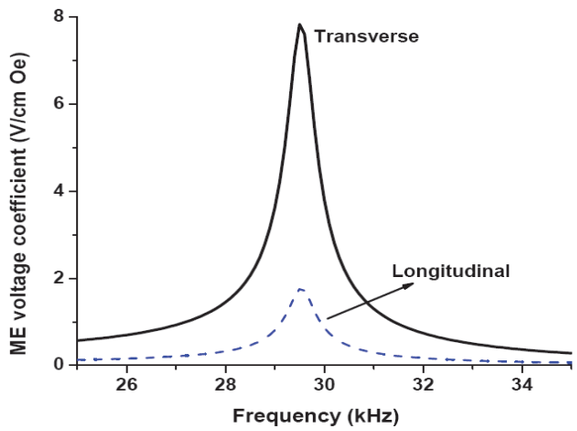

Fig. 2. Frequency dependence of longitudinal and transverse ME voltage coefficients for a bilayer of permendur and PZT showing the resonance enhancement of ME interactions at the bending mode frequency. The bilayer is free to bend at both ends. The sample dimensions are L = 9.2 mm and total thickness t = 0.7 mm and the PZT volume fraction v=0.6.

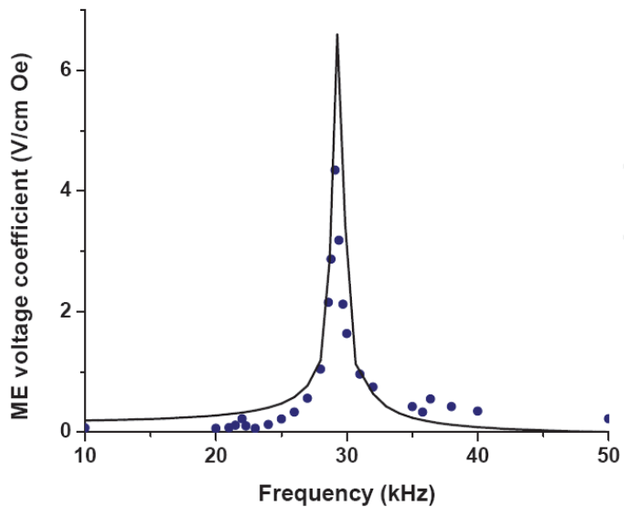

Fig. 3. Theoretical (line) and measured (circles) frequency dependence of transverse ME voltage coefficients for a permendur-PZT bilayer that is free to bend at both ends and with v=0.67.

5. Inverse magnetoelectric effect

In the case of inverse ME effect, external field E produces a deformation of piezoelectric layers due to piezoelectric coupling. The deformation is transmitted to magnetic layers. The inverse piezomagnetic effect results in a change of magnetic parameters of the structure. ME coefficient $a_{H,\,ij}=H_i/E_j$ can be easily found similarly to ME voltage coefficient using the open magnetic circuit condition, $B_i=0$. As an example, the expression for $a_{H,\,33}$ takes the form (Huang, 2006)

$$\alpha_{H,33} = \frac{-2d_{31}q_{31}{}^{m}v}{({}^{m}s_{11}^{H} + {}^{m}s_{12}^{H})^{p}v + (ps_{11}^{E} + {}^{p}s_{12}^{E})^{m}v - 2(k_{31})^{2}\,{}^{p}s_{11}^{E}\,{}^{m}v}, \tag{13}$$

where k_{31} is the coupling coefficient for the piezoelectric phase, ${}^{p}v$ and ${}^{m}v$ are the volume fractions of piezoelectric and magnetostrictive components.

5.1 Inverse magnetoelectric effect at electromechanical resonance

To obtain the inverse ME effect, a pick up coil wound around the sample is used to measure the ME voltage due to the change in the magnetic induction in magnetostrictive phase. The measured static magnetic field dependence of ME voltage has been attributed to the variation in the piezomagnetic coefficient for magnetic layer. The frequency dependence of the ME voltage shows a resonance character due to longitudinal acoustic modes in piezoelectric layer. Next we derive an expression for the ME susceptibility at EMR. (Fetisov et al., 2007) For the transverse field orientation, the equations for the strain tensor S_i in the ferrite and piezoelectric and the magnetic induction B have the form

$$\begin{aligned} {}^{p}S_1 &= {}^{p}s_{11}{}^{p}T_1 + {}^{p}d_{31}E_3, \\ {}^{m}S_1 &= {}^{m}s_{11}{}^{m}T_1 + {}^{m}g_{11}B_1, \end{aligned} \tag{14}$$

$${}^{m}H_1 = B_1 / {}^{m}\mathrm{m}_{33} - {}^{m}g_{11}{}^{m}T_1, \tag{15}$$

where ps11 and ms11are the components of the compliance tensor at constant electric field for piezoelectric and at constant magnetic induction for ferrite, respectively; ${}^{m}\mu_{33}$ is the component of the permeability tensor, and ${}^{p}d_{31}$ and ${}^{m}q_{11}$ are the piezoelectric and piezomagnetic coefficients, respectively. Here we take into account only stress components along x axis, because close to EMR we can assume $T_1 >> T_2$ and T_3. Expressing the stress components via the deformation components and substituting these expressions into the equation of the medium motion, we obtain a differential equation for the x projection of the displacement vector of the medium (u_x). Taking into account the fact that the trilayer surfaces at $x=0$ and $x=L$ are free from external stresses, we find the solution to this equation. The magnetic induction arising due to the piezoelectric effect can be found from Eq. 15. The magnetic induction in the trilayer is expressed as:

$$B_1 = {}^{m}\mu_{33}\int_0^L ({}^{m}H_1 + {}^{m}g_{11}{}^{m}T_1)dx, \tag{16}$$

where W and L are the width and length of the sample. The ME susceptibility is defined by $\alpha_{31} = \frac{\partial B_1}{\partial E_3}$. Taking into account this definition, Eq. 16 yields:

$$\alpha_{31} = \frac{2v(1-v)^{m}q_{11}\,{}^{p}d_{31}\tan(kL/2)}{kL[v^{m}s_{11} + (1-v)^{p}s_{11}]} \tag{17}$$

where $k = \omega\sqrt{\left[{}^{p}\rho\, v + {}^{m}\rho(1-v)\right]\left[\frac{v}{{}^{p}s_{11}} + \frac{1-v}{{}^{m}s_{11}}\right]^{-1}}$, v is the PZT volume fraction and ρ is average density. Eq. 17 does not take into account power waste therefore at resonant frequency the ME coefficient sharply increases. In real structures, there are losses that occur first of all in the contacts. These losses can be taken into account in Eq. 17 by substituting ω for $\omega' - i\omega''$ with $\omega''/\omega' = 1/Q$ where Q is the measured quality factor of EMR. The estimated the ME susceptibility is shown in Fig. 5. The susceptibility determined from data on generated magnetic induction at opened magnetic circuit is also shown in Fig. 5. One observes a very good agreement between theory and data. The investigations carried out have enabled us to establish a relation between efficiencies of the direct and the inverse ME interactions and their frequency dependences.

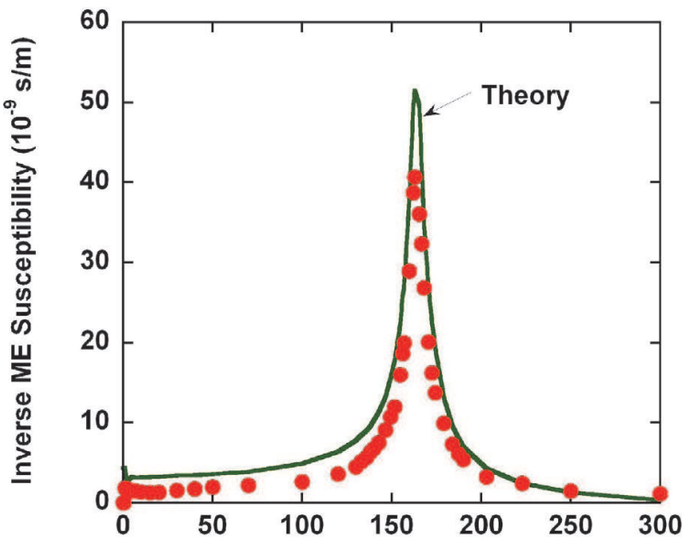

Fig. 4. Theoretical (line) and measured (filled circles) ME susceptibility for the PZT-Ni-PZT trilayer structure.

5.2 Inverse magnetoelectric effect at microwave range

A thorough understanding of high frequency response of a ferrite - piezoelectric composite is critically important for a basic understanding of ME effects and for useful technologies. In a composite, the interaction between electric and magnetic subsystems can be expressed in terms of a ME susceptibility. In general, the susceptibility is defined by the following equations for the microwave region (Kornev et al., 2000; Bichurin, 1994; Bichurin et al., 1990).

$$\begin{aligned} \mathbf{p} &= \chi^{E}\mathbf{e} + \chi^{EM}\mathbf{h}, \\ \mathbf{m} &= \chi^{ME}\mathbf{e} + \chi^{M}\mathbf{h}. \end{aligned} \tag{18}$$

Here **p** is the electrical polarization, **m** is the magnetization, **e** and **h** are the external electrical and magnetic fields, χ^E and χ^M are the electrical and magnetic susceptibilities, and χ^{EM} and χ^{ME} are the ME susceptibilities , with $\chi_{ik}^{ME} = \chi_{ki}^{EM}$. In Eq. 18, the ac amplitudes are shown explicitly, but the susceptibilities also depend on constant fields.

We consider the magnetic susceptibility tensor of a composite which exhibits ME coupling. The sample is subjected to constant electric and magnetic fields and a ac magnetic field. The thermodynamic potential density can be written as:

$$W = W_0 + W_{ME}, \tag{19}$$

where W_0 is the thermodynamic potential density at $\boldsymbol{E} = 0$, and

$$W_{ME} = B_{ikn}E_iM_kM_n + b_{ijkn}E_iE_jM_kM_n\,. \tag{20}$$

Here B_{ikn} and b_{ijkn} are linear and bilinear ME constants, respectively. The number of independent components is determined by the material structure. The main contribution to W_{ME} arises from the linear ME constants B_{ikn} in polarized composites. If the composite is unpolarized, the bilinear ME constants is dominant. We used the effective demagnetization factor method to solve the linearized equation of motion of magnetization and obtained the following expression for the magnetic susceptibility:

$$\chi^M = \begin{bmatrix} \chi_1 & \chi_s + i\chi_a & 0 \\ \chi_s - i\chi_a & \chi_2 & 0 \\ 0 & 0 & 0 \end{bmatrix}, \tag{21}$$

where

$$\chi_1 = D^{-1}\gamma^2 M_0\Big[H_{03'} + M_0\sum_i (N_{2'2'}{}^i - N_{3'3'}^i)\Big];\ \chi_2 = D^{-1}\gamma^2 M_0[H_{03'} + M_0\sum_i (N_{1'1'}^i - N_{3'3'}^i)];$$

$$\chi_s = -D^{-1}\gamma^2 M_0^2\sum_i N_{1'2'}^i;\ \chi_a = D^{-1}\gamma M_0\omega;\ D = \omega_0^2 - \omega^2;$$

$$\omega_0^2 = \gamma^2[H_{03'} + \sum_i (N_{1'1'}^i - N_{3'3'}^i)M_0][H_{03'} + \sum (N_{2'2'}^i - N_{3'3'}^i)M_0] - (\sum_i N_{1'2'}^i M_0)^2$$

Here γ is the magneto-mechanical ratio, ω is the angular frequency, $N_{k'n'}^i$ are demagnetization factors describing the effective magnetic anisotropy fields, and $1',2',3'$ is a coordinate system in which the axis $3'$ is directed along the equilibrium magnetization. In Eq. 21 the summation is carried out over all types of magnetic anisotropy. The ME interaction results in an additional term (i =E)

$$N_{k'n'}^E = 2(B_{ikn} + b_{ijkn}E_{oj})E_{oi}\beta_{k'k}\beta_{n'n}, \tag{22}$$

where $\boldsymbol{\beta}$ is matrix of direction cosines of axes $(1',2',3')$ relative to the crystallographic coordinate system (1, 2, 3). It should be noted that $\chi_{33}^M = 0$ in Eq. 21 since the sample is supposed to be magnetized by bias field that is high enough to drive the composite to a saturated (single-domain) state. Using Eq. 21 it can be easily shown that the resonance line shift under the influence of the electric field to the first order in N_{kl}^E has the form:

$$\delta H_E = -\frac{M_0}{Q_1}\left[Q_2\left(N_{11}^E - N_{33}^E\right) + Q_3\left(N_{22}^E - N_{33}^E\right) - Q_4 N_{12}^E \right], \tag{23}$$

where

$$Q_1 = 2H_3 + M_0\sum_{i\neq E}\left[\left(N_{11}^E - N_{33}^E\right) + \left(N_{22}^E - N_{33}^E\right)\right];\ Q_2 = \left[H_3 + M_0\sum_{i\neq E}\left(N_{22}^E - N_{33}^E\right)\right];$$

$$Q_3 = \left[H_3 + M_0\sum_{i\neq E}\left(N_{11}^E - N_{33}^E\right)\right];\ Q_4 = 2M_0\sum_{i\neq E} N_{12}^i\ .$$

Eq. 23 enables us to determine the ME constants of a composite and consequently to interpret the obtained data on the resonant ME effect. As an example, we consider the composite with *3m* or *4mm* symmetry. The general expression for the magnetic susceptibility tensor of a disk sample magnetized along the symmetry axis has the form

$$\chi_1 = \chi_2 = D^{-1}\gamma^2 M_0 H_{eff};\ \chi_s = 0;\ \chi_a = D^{-1}\gamma M_0\omega, \tag{24}$$

where

$$D = \omega_0^2 - \omega^2;\ \omega_0 = \gamma\ H_{eff};\ H_a = K_1 / M_0;$$

$$H_{eff} = H_0 + 2H_a - 4\pi M_0 + 2M_0(B_{31} - B_{33})E_0 + 2M_0(b_{31} - b_{33})E_0^2$$

Assuming the dissipative term in the equation of motion of magnetization as $i\omega\alpha(\mathbf{M_0}\times\mathbf{m})/M_0$, where α is the dissipation parameter, the magnetic susceptibility tensor components are complex and take the form $\chi_1 = \chi' + i\,\chi''$, where

$$\chi' = \chi_0\ \frac{\omega_0^2\left(\omega_0^2 - \omega^2 + 2\alpha^2\omega^2\right)}{\left(\omega_0^2 - \omega^2\right)^2 + 4\alpha^2\omega_0^2\omega^2},\ \chi'' = \chi_0\ \frac{\alpha\omega\omega_0\left(\omega_0^2 + \omega^2\right)}{\left(\omega_0^2 - \omega^2\right)^2 + 4\alpha^2\omega_0^2\omega^2},\ \chi_0\ = \gamma\frac{M_0}{\omega_0}. \tag{25}$$

It follows from Eqs. 21 and 24 that the dependence of the magnetic susceptibility on an external constant electric field is resonant. The nature of this dependence can be explained as follows. By means of ME interactions, the external electric field results in a change in the effective magnetic field H_{eff} in Eq. 24 with $2H_{ME} = 2M_0(B_{31} - B_{33})E_0 + 2M_0(b_{31} - b_{33})E_0^2$. The change originates from the piezoelectric phase mechanically coupled to the magnetostrictive phase, and is phenomenological described by ME constants B_{ikn} and b_{ijkn} in Eqs. 28 and 29. Thus the variation of the external constant electric field has the same effect as magnetic field variations and reveals a resonant behavior. Expressions for the susceptibility components could be obtained by using the demagnetization factors stipulated by ME interactions according to Eq. 26.

Next we consider specific composites and estimate the magnetic susceptibility and its electric field variation. (Bichurin et al., 2002) Three composites of importance for the estimation are lithium ferrite (LFO) - PZT, nickel ferrite (NFO) - PZT and yttrium iron garnet (YIG) - PZT because of desirable high frequency properties of LFO, NFO and YIG. We consider a simple structure, a bilayer consisting of single ferrite and PZT layers. In order to obtain the susceptibilities, one requires the knowledge of ME constants and the

loss parameter. Assuming that the poling axis of the piezoelectric phase coincides with [100] axis of the magnetostrictive phase and $|\lambda_{100}| = 1.4 \cdot 10^{-6}$, $23 \cdot 10^{-6}$ and $46 \cdot 10^{-6}$ for YIG-PZT, LFO-PZT and NFO-PZT, respectively, we obtained $2M_0(B_{31}-B_{33}) = 0.1$, 0.6 and 1.4 *Oe·cm/kV* for the three bilayer samples. For LFO the following parameters are used: ${}^m c_{11} = 24.47 \cdot 10^{10}$ *N/m²*; ${}^m c_{12} = 13.71 \cdot 10^{10}$ *N/m²*; ${}^m c_{44} = 9.36 \cdot 10^{10}$ *N/m²*; $4\pi M_s = 3600$ *G*. Finally, the loss parameters are $\alpha = 0.025$, 0.05 *and* 0.075 for YIG-PZT, LFO-PZT and NFO-PZT, respectively. Figure 5 shows the static magnetic field dependencies of real and imaginary parts of magnetic susceptibility for layered LFO-PZT, NFO– PZT and YIG – PZT. The results are for a bilayer disk sample with the H and E-fields perpendicular to the sample plane and for a frequency of 9.3 GHz. The static field range is chosen to include ferromagnetic resonance in the ferrite. For E = 0, one observes the expected resonance in the profiles. With the application of E = 300 kV/cm, a down-shift in the resonance field is obvious. The magnitude of the shift is determined by ME constants which in turn is strongly influenced by the magnetostriction constant. The large magnetostriction for NFO leads to a relatively strong E-induced effect in NFO-PZT compared to YIG-PZT. The shift also correlates with resonance linewidth. It is possible to understand the correlation from the fact that the resonance linewidth is dependent on the effective anisotropy field, a parameter that is a function of the magnetostriction.

Figure 6 shows the estimated variation of the real and imaginary parts of the magnetic susceptibility as a function of E for a frequency of 9.3 GHz. The constant magnetic field is set equal to the field for ferromagnetic resonance (FMR). The width of resonance measured in terms of electric field is inversely proportional to the parameter $2M_0(B_{31}-B_{33})$. It follows from Eq. 29 that a narrow resonance is indicative of strong ME coupling in the composites. Thus NFO-PZT bilayer shows a sharp resonance in comparison to YIG-PZT.

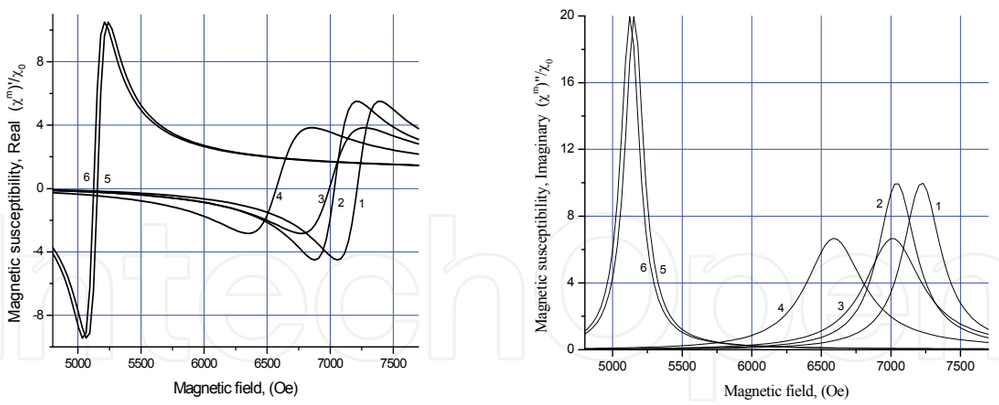

(a) (b)

Fig. 5. Theoretical magnetic field dependence of the magnetic susceptibility for the multilayer composites of LFO-PZT (curves 1 and 2), NFO– PZT (curves 3 and 4) and YIG–PZT (curves 5 and 6) represents the real (a) and imaginary (b) parts of the susceptibility at 9.3 GHz. Curves 1, 3 are at E=0 and curves 2, 4 at E=300 kV/cm.

Figures 5 and 6 represent the magnetic spectra of the composites obtained by magnetic and electric sweep, respectively. Thus the presented model enables finding ME coefficients from data on the electric field induced shift of magnetic resonance line.

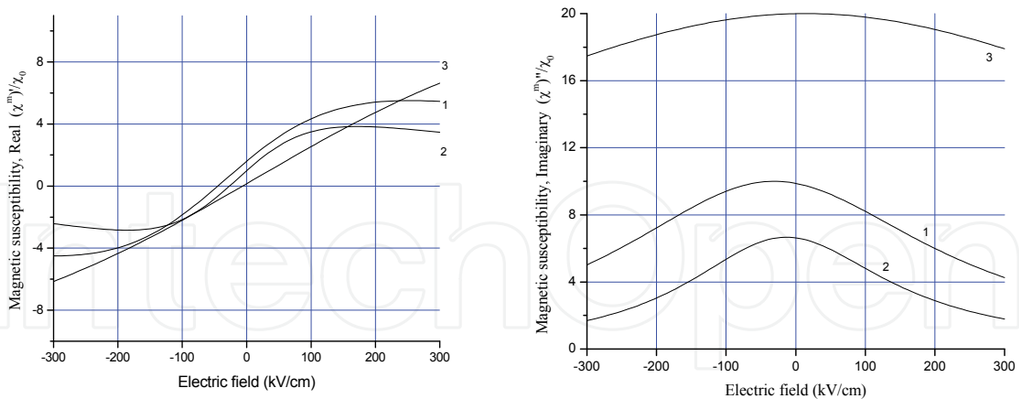

(a) (b)

Fig. 6. Theoretical electric field dependence of the magnetic susceptibility for the multilayer composites of LFO-PZT (curves 1), NFO– PZT (curve 2) and YIG– PZT (curve 3) represents the real (a) and imaginary (b) parts of the susceptibility at 9.3 GHz.

6. Magnetoelectric coupling in magnetoacoustic resonance region

Here we provide a theory for ME interactions at the coincidence of FMR and EMR, at magnetoacoustic resonance (MAR). (Bichurin et al., 2005; Ryabkov et al., 2006) At FMR, spin-lattice coupling and spin waves that couple energy to phonons through relaxation processes are expected to enhance the piezoelectric and ME interactions. Further strengthening of ME coupling is expected at the overlap of FMR and EMR. We consider bilayers with low-loss ferrites such as nickel ferrite or YIG that would facilitate observation of the effects predicted in this work. For calculation we use equations of motion for the piezoelectric and magnetostrictive phases and equations of motion for the magnetization. Coincidence of FMR and EMR allows energy transfer between phonons, spin waves and electric and magnetic fields. This transformation is found to be very efficient in ferrite-PZT. The ME effect at MAR can be utilized for the realization of miniature/nanosensors and transducers operating at high frequencies since the coincidence is predicted to occur at microwave frequencies in the bilayers.

We consider a ferrite-PZT bilayer that is subjected to a bias field H_0. The piezoelectric phase is electrically polarized with a field E_0 parallel to H_0. It is assumed that H_0 is high enough to drive the ferrite to a saturated (single domain) state that has two advantages. When domains are absent, acoustic losses are minimum. The single-domain state under FMR provides the conditions necessary for achieving a large effective susceptibility. The free-energy density of a single crystal ferrite is given by ${}^mW = W_H + W_{an} + W_{ma} + W_{ac}$, where $W_H = - \boldsymbol{M} \cdot \boldsymbol{H_i}$ is Zeeman energy, M is magnetization, H_i is internal magnetic field that includes demagnetizing fields. The term W_{an} given by $W_{an} = K_1/M_0^4(M_1^2 M_2^2 + M_2^2 M_3^2 + M_3^2 M_1^2)$ with K_1 the cubic anisotropy constant and M_0 the saturation magnetization. The magnetoelastic energy is written as $W_{ma} = B_1/M_0^2 (M_1^2 {}^mS_1 + M_2^2 {}^mS_2 + M_3^2 {}^mS_3) + B_2/M_0^2(M_1 M_2 {}^mS_6 + M_2 M_3 {}^mS_4 + M_1 M_3 {}^mS_5)$ where B_1 and B_2 are magnetoelastic coefficients and S_i are the elastic coefficients. Finally, the elastic energy is $W_{ac} = \frac{1}{2} {}^mc_{11}({}^mS_1^2 + {}^mS_2^2 + {}^mS_3^2) + \frac{1}{2} {}^mc_{44} ({}^mS_4^2 + {}^mS_5^2 + {}^mc_{12} ({}^mS_1 {}^mS_2 + {}^mS_2 {}^mS_3 + {}^mS_1 {}^mS_3)$ and ${}^mc_{ij}$ is modulus of elasticity.

The generalized Hook's law for the piezoelectric phase can be presented as follows.

$$
\begin{aligned}
{}^{p}T_4 &= {}^{p}c_{44}\,{}^{p}S_4 - {}^{p}e_{15}\,{}^{p}E_2, \\
{}^{p}T_5 &= {}^{p}c_{44}\,{}^{p}S_5 - {}^{p}e_{15}\,{}^{p}E_1,
\end{aligned}
\tag{26}
$$

where e_{p15} is piezoelectric coefficient and ${}^{p}E$ is electric field. Equations of motion for ferrite and piezoelectric composite phases can be written in following form:

$$
\begin{aligned}
&\partial^2\left({}^{m}u_1\right)/\partial t^2 = \partial^2\left({}^{m}W\right)/\left(\partial x\partial {}^{m}S_1\right) + \partial^2\left({}^{m}W\right)/\left(\partial y\partial {}^{m}S_6\right) + \partial^2\left({}^{m}W\right)/\left(\partial z\partial {}^{m}S_5\right), \\
&\partial^2\left({}^{m}u_2\right)/\partial t^2 = \partial^2\left({}^{m}W\right)/\left(\partial x\partial {}^{m}S_6\right) + \partial^2\left({}^{m}W\right)/\left(\partial y\partial {}^{m}S_2\right) + \partial^2\left({}^{m}W\right)/\left(\partial z\partial {}^{m}S_4\right), \\
&\partial^2\left({}^{p}u_1\right)/\partial t^2 = \partial\left({}^{p}T_1\right)/\partial x + \partial\left({}^{p}T_6\right)/\partial y + \partial\left({}^{p}T_5\right)/\partial z, \\
&\partial^2\left({}^{p}u_2\right)/\partial t^2 = \partial\left({}^{p}T_6\right)/\partial x + \partial\left({}^{p}T_2\right)/\partial y + \partial\left({}^{p}T_4\right)/\partial z.
\end{aligned}
\tag{27}
$$

The equation of motion of magnetization for ferrite phase has the form

$$
\partial \mathbf{M}/\partial t = -\gamma\left[\mathbf{M}, \mathbf{H}_{\mathbf{eff}}\right], \tag{28}
$$

where $\boldsymbol{H_{eff}} = -\partial({}^{m}W)/\partial \boldsymbol{M}$. Solving Eqs. 31 and 32, taking into account Eq. 30 and open circuit condition, allows one to get the expression for ME voltage coefficient

$$
\begin{aligned}
&\left|\alpha_E\right| = \left|E^+ / H^+\right| = \gamma B_2\, {}^{p}c_{44}\,{}^{p}k\,{}^{p}e_{15}\,(1-cos({}^{p}k\,{}^{p}L)(1-cos\left({}^{m}k\,{}^{m}L\right. / \{(\omega - \gamma H_0 + 4\pi\,\gamma M_0\right) \\
&[{}^{p}k\,{}^{p}c_{44} cos({}^{m}k_m\,{}^{m}L)(2\,{}^{p}e_{15}{}^{2}(1-cos({}^{p}k\,{}^{p}L) + sin({}^{p}k\,{}^{p}L)\,{}^{p}c_{44}\,{}^{p}\varepsilon_{11}\,{}^{p}k\,{}^{p}L) + \\
&+ {}^{m}k\,{}^{m}c^{+}{}_{44} sin({}^{m}k\,{}^{m}L)({}^{p}e_{15}{}^{2} sin({}^{p}k\,{}^{p}L) + cos({}^{p}k\,{}^{p}L)\,{}^{p}c_{44}\,{}^{p}\varepsilon_{11}\,{}^{p}k\,{}^{p}L)]\},
\end{aligned}
\tag{29}
$$

where ${}^{m}k = \omega\sqrt{{}^{m}\rho({}^{m}c_{44}^{+})^{-1}}$, ${}^{p}k = \omega\sqrt{{}^{p}\rho({}^{p}c_{44})^{-1}}$, $H^+ = H_1 + i\,H_2$, $E^+ = E_1 + i\,E_2$. Now we apply the theory to specific bilayer system of YIG-PZT. YIG has low-losses at FMR, a necessary condition for the observation of the enhancement in ME coupling at MAR that is predicted by the theory. The assumed thicknesses for YIG and PZT are such that the thickness modes occur at 5-10 GHz, a frequency range appropriate for FMR in a saturated state in YIG. The resonance field H_r is given by $H_r = \omega/\gamma - 4\pi M_o$. As H_0 is increased to H_r, α_E is expected to increase and show a resonant character due to the resonance form for frequency dependence for mechanical displacement in the FMR region. Figure 7 shows estimated α_E vs f. Signal attenuation is taken into account in these calculations by introducing a complex frequency and for an imaginary component of $\omega = 10^7$ rad/s.

7. Lead-free ceramic for magnetoelectric composites

Owing to the prohibition on the use of Pb-based materials in some commercial applications the demand for lead-free ceramics has grown considerably in the last decade. Various systems for nonlead ceramics have been studied and some of these have been projected as the possible candidates for the replacement of PZT. However, the dielectric and piezoelectric properties of all the known nonlead materials is inferior as compared to that PZT and this has been the stimulant for growing research on this subject. For high piezoelectric properties perovskite is the preferred crystallographic family and large piezoelectric and electromechanical constants are obtained from alkali-based ceramics such

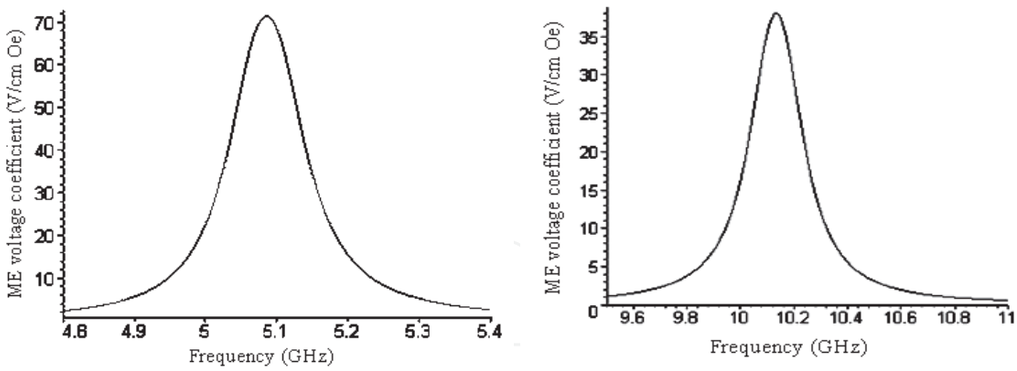

(a) (b)

Fig. 7. The ME voltage coefficient a_E vs. frequency profile for a bilayer of PZT of thickness 100 nm and YIG of thickness 195 nm and for dc magnetic field of 3570 (a) and 5360 (b) Oe. The FMR frequency coincides with fundamental EMR mode (a) and second EMR mode (b) frequency.

as $(Na_{1/2}Bi_{1/2})TiO_3$ (NBT), $(K_{1/2}Bi_{1/2})TiO_3$ (KBT) and $(Na_{0.5}K_{0.5})NbO_3$. Table VII.1 compares the properties of the PZT and the prominent non-lead based systems. The data shown in this table has been collected from various publications (Nagata & Takenaka, 1991; Sasaki et al., 1999; Kimura et al., 2002; Priya et al., 2003a, 2003b). It can be easily deduced from the data shown in this table that none of the nonlead ceramics qualifies for the direct replacement of PZT. (Na, K)NbO_3 ceramics has good longitudinal mode and radial mode coupling factors along with high piezoelectric constants.

	Symbol	$\varepsilon_{33}^T/\varepsilon_0$	Qm	d_{33} (pC/N)	d_{31} (pC/N)	k_{33} (%)	k_p (%)	Tc (°C)
PZT (Mn, Fe doped)	PZT	1500	1000-2000	300	-100	60	50	300
$(Bi,Na)TiO_3$	BNT(1)	600	500	120	-40	45	25	260
Bi-layer	SBT(1)	150	>2000	20	-3	20	3	550
	NCBT(1)	150	–	15	-2	15	2	>500
	NCBT(1)(HF(2), TGG(2))	150	–	40	-2	40	2	>500
(Na,K)NbO_3	KNN(1)	400	500	120	-40	40	30	350
Tungsten Bronze	SBN(1)	500	–	120	–	30	–	250
Others	BT(1)	1100	700	130	-40	45	20	100

Table 1. Properties of lead-free piezoelectric ceramics. (1) BNT: $(Bi_{1/2}\ Na_{1/2})TiO_3$, SBT: $SrBi_4Ti_4O_{15}$, NCBT: $(Na_{1/2}Bi_{1/2})_{0.95}Ca_{0.05}Bi_4Ti_4O_{15}$, KNN: $(K_{1/2}Na_{1/2})NbO_3$, SBN: $(Sr,Ba)Nb_2O_6$, BT: $BaTiO_3$; (2) HF: Hot Forging method, TGG: Templated grain growth method.

It is well known that the composition corresponding to 0.5/0.5 in the $NaNbO_3$ – $KNbO_3$ (KNN) system has the maximum in the piezoelectric properties. Table VII.2 compares the properties of the annealed and un-annealed KNN samples. KNN has an intermediate phase transition from the ferroelectric orthorhombic phase (FE_o) to the ferroelectric tetragonal phase (FE_t) at around 200 ^oC. It is believed that annealing the sample in the tetragonal phase induces (100) oriented domains at room temperature. Since the spontaneous polarization is along <110> in the orthorhombic phase, rapid cooling (100^{o}C/min) from FE_t phase (spontaneous polarization along <100>) results in titling of the polarization which provides enhancement of piezoelectric properties.

Sintering Temperature (^oC)	Density (gm/cm^3)	Logρ (Ω.cm)	tanδ (%)	ε
1150	4.23	9.4	10	720
1160 (Annealed)	4.44	9.97	4.05	616
1160 (Unannealed)	4.45	10.14	4.75	630

Table 2. Properties of unpoled KNN ceramics showing the affect of annealing.

Figure 8 (a) and (b) shows the dielectric constant and loss as a function of temperature for the poled KNN sample. The room temperature dielectric constant is of the order of 350. The dielectric constant curve shows a discontinuity at ~180 ^oC and 400 ^oC. These discontinuities are related to the transition from FE_o phase to FE_t phase and FE_t phase to PE_c. In the range of 0 – 180 ^oC, the dielectric loss magnitude remains in the range of 4.2 – 4.5%. No significant difference was observed in the dielectric behavior of the annealed and unannealed samples below 200 ^oC.

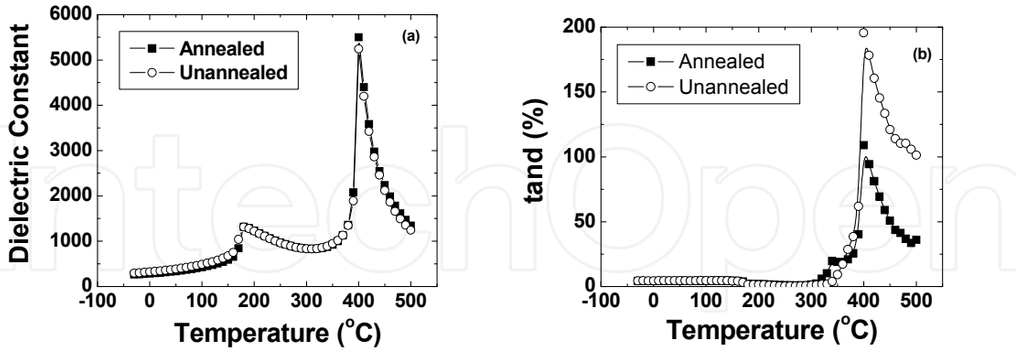

(a) (b)

Fig. 8. Temperature dependence of dielectric constant and loss for KNN. (a) Dielectric constant and (b) Dielectric loss.

The magnitude of piezoelectric constants at room temperature for annealed samples was found to be: d_{33} = 148 pC/N and d_{31} = 69 pC/N. The magnitude of d_{33} for the unannealed sample was found to be 119 pC/N. Figure 9 (a) and (b) shows the radial mode electromechanical coupling factor (k_p) and mechanical quality factor (Q_m) as a function of

temperature. It can be clearly seen that piezoelectric properties remain almost constant until the FE_t phase appears at 180 ^oC. The magnitude of k_p at room temperature is of the order of 0.456 and Q_m is around 234. Since in this system the high temperature phase (FE_t) is also ferroelectric there is no danger of depoling on exceeding the transition temperature. This provides a considerable advantage over the competing NBT-KBT and NBT-BT systems and for this reason KNN ceramics are the most promising high piezoelectric non-lead system.

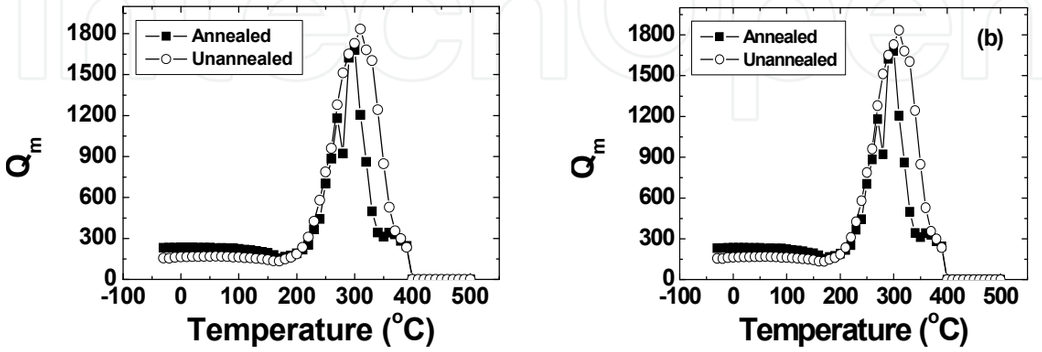

Fig. 9. Temperature dependence of piezoelectric properties for KNN. (a) Radial mode coupling factor and (b) Mechanical quality factor.

Further improvement in the properties of KNN can be obtained by synthesizing solid solution (1-x)$(Na_{0.5}K_{0.5})NbO_3$-x$BaTiO_3$. Three phase transition regions exist in (1-x)$(Na_{0.5}K_{0.5})NbO_3$-x$BaTiO_3$ ceramics corresponding to orthorhombic, tetragonal, and cubic phases. The composition 0.95$(Na_{0.5}K_{0.5})NbO_3$-0.05$BaTiO_3$, which lies on boundary of orthorhombic and tetragonal phase, was found to exhibit excellent piezoelectric properties. The piezoelectric coefficients of this composition were measured on a disk-shaped sample and were found to be as following: k_p=0.36, d_{33}=225 pC/N and $\varepsilon_{33}^T/\varepsilon_0$=1058 (Ahn et al., 2008). The properties of this composition were further improved by addition of various additives making it suitable for multilayer actuator application. The composition 0.06$(Na_{0.5}K_{0.5})NbO_3$-0.94$BaTiO_3$ was found to lie on the boundary of tetragonal and cubic phase. This composition exhibited the microstructure with small grain size and excellent dielectric properties suitable for multi-layer ceramic capacitor application. Table 3 shows the piezoelectric properties of modified 0.95$(Na_{0.5}K_{0.5})NbO_3$-0.05$BaTiO_3$ (KNN-BT) ceramics. It can be seen from this table that excellent piezoelectric properties with high transitions temperatures can be obtained in this system making it a suitable candidate for lead – free magnetoelectric composite.

The choice for the magnetostrictive phase in sintered or grown composites is spinel ferrites. In the spinel ferrites, the spontaneous magnetization corresponds to the difference between the sublattice magnetizations associated with the octahedral and tetrahedral sites. Results have shown enhanced magnitude of the ME coefficient for $Ni_{0.8}Zn_{0.2}Fe_2O_4$ (NZF) and $Co_{0.6}Zn_{0.4}Fe_2O_4$ (CZF). In the nickel zinc ferrite solid solution ($Ni_{1-x}Zn_xFe_2O_4$) as x is increased Zn^{2+} replaces Fe^{3+} in the tetrahedral sites and Fe^{3+} fills the octahedral sites emptied by Ni^{2+}. The net magnetization of nickel zinc ferrite is proportional to 5(1 + x) + 2(1 - x) - 0(x) - 5(1 - x) = 2 + 8x**.** Thus, the magnetic moment as a function of the Zn content increases until

there are so few Fe^{3+} ions remaining in tetrahedral sites that the superexchange coupling between tetrahedral and octahedral sites breaks down. Figure 10 shows our results on the PZT – NZF and PZT – CZF composites. It can be seen from this figure that CZF is a hard magnetic phase, requires higher DC bias, has lower remanent magnetization and results in larger reduction of the ferroelectric polarization as compared to NZF. On the other hand, a high increase in the resistivity of the Ni-ferrites is obtained by doping with Co. Thus, a combination of NZF and modified KNN-BT phase presents an opportunity to develop magnetoelectric composites with reasonable magnitude of coupling coefficient. Figure 11 (a) and (b) shows the ME response of (1-x) [$0.948K_{0.5}Na_{0.5}NbO_3$ – $0.052LiSbO_3$] – x $Ni_{0.8}Zn_{0.2}Fe_2O_4$ (KNNLS-NZF) composites. A reasonable magnitude of ME coefficient was obtained for the sintered composites (Yang et al., 2011). Compared to PZT based ceramics, this magnitude is about 50% smaller in magnitude.

Additives (in 0.95NKN-0.05BT)	d_{33} (pC/N)	k_p	$\varepsilon_3^T/\varepsilon_0$	Q_m	T_c (^oC)	Sin. T. (^oC)
None [40,41]	225	0.36	1,058	74	320	1,060
0.5 mol% MnO_2 [53]	237	0.42	1,252	92	294	1,050
1.0 mol% ZnO	220	0.36	1,138	71	-	1,040
2.0 mol% CuO [47,54]	220	0.34	1,282	186	286	950
2.0 mol% CuO + 0.5 mol% MnO_2 [54]	248	0.41	1,258	305	277	950

Table 3. Piezoelectric and dielectric properties of $0.95(Na_{0.5}K_{0.5})$-$0.05BaTiO_3$ + additives.

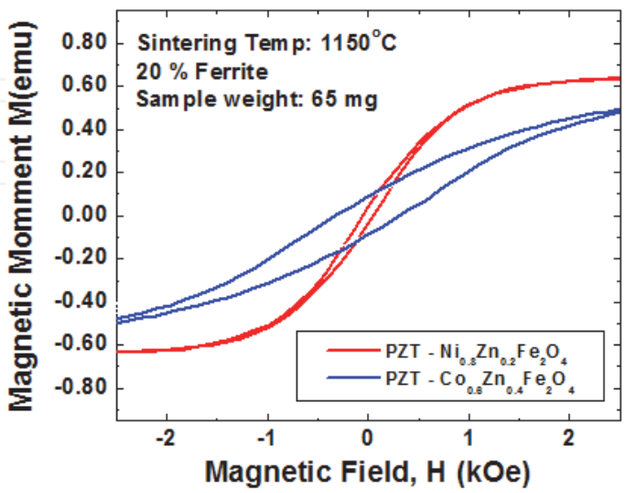

Fig. 10. Comparison of magnetic properties for *PZT-NZF and PZT-CZF.*

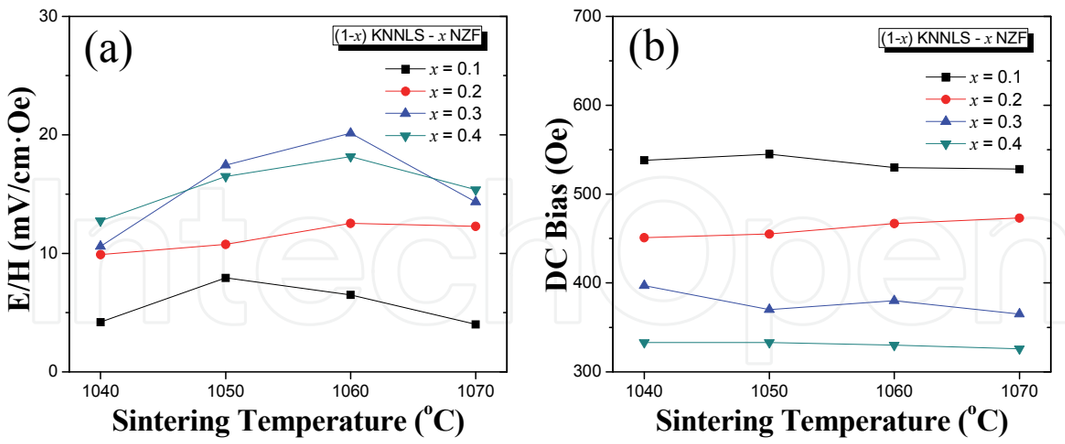

Fig. 11. ME coefficient and H_{bias} for (1-x) KNNLS – x NZF composites.

8. Devices based on magnetoelectric interactions

8.1 Ac magnetic field sensors

The working principle of magnetic sensing in the ME composites is simple and direct. (Nan et al., 2008) When probing a magnetic field, the magnetic phase in the ME composites strains, producing a proportional charge in the piezoelectric phase.

Highly sensitive magnetic field sensors can be obtained using the ME composites with high ME coefficients. The ME composites can be used as a magnetic probe for detecting ac or dc fields.

Apart from a bimorph, a multilayer configuration of ME laminates has been reported that enables ultralow frequency detection of magnetic field variations. This configuration can greatly improve the low-frequency capability because of its high ME charge coupling and large capacitance. At an extremely low frequency of f =10 mHz, the multilayer ME laminates can still detect a small magnetic field variation as low as 10^{-7} T.

8.2 Magnetoelectric gyrators

ME transformers or gyrators have important applications as voltage gain devices, current sensors, and other power conversion devices. An extremely high voltage gain effect under resonance drive has been reported in long-type ME laminates consisting of Terfenol-D and PZT layers. A solenoid with n turns around the laminate that carries a current of Iin was used to excite a H_{ac}. The input ac voltage applied to the coils was V_{in}. When the frequency of H_{ac} was equal to the resonance frequency of the laminate, the magnetoelectric voltage coefficient was strongly increased, and correspondingly the output ME voltage (V_{out}) induced in the piezoelectric layer was much higher than V_{in}. Thus, under resonant drive, ME laminates exhibit a strong voltage gain, offering potential for high-voltage miniature transformer applications. Figure 12 shows the measured voltage gain Vout $/ V$in as a function of the drive frequency for a ME transformer consisting of Terfenol-D layers of 40 mm in length and a piezoelectric layer of 80 mm in length. A maximum voltage gain of 260 was found at a resonance frequency of 21.3 kHz. In addition, at the resonance state, the maximum voltage gain of the ME transformer was strongly dependent on an applied H_{dc},

which was due to the fact that Terfenol-D has a large effective piezomagnetic coefficient only under a suitable H_{dc}. Other reports have shown that a ME laminate with a coil carrying current *I*in has a unique current-to-voltage *I-V* conversion capability. ME laminates actually act as a *I-V* gyrator, with a high *I-V* gyration coefficient (Dong et al., 2006a; Zhai et al., 2006). Fig. 13 shows ME gyration equivalent circuit. At electromechanical resonance, the ME gyrator shows a strong *I-V* conversion of 2500 V/A, as shown in Fig. 10.
We also observed (i) reverse gyration: an input current to the piezoelectric section induced a voltage output across coils, and (ii) impedance inversion: a resistor *Ri* connected in parallel to the primary terminals of the gyrator resulted in an impedance G_2 /*Ri* in series with the secondary terminals.

8.3 Microwave devices

Ferrite–ferroelectric layered structures are of interest for studies on the fundamentals of high-frequency ME interaction and for device technologies. Such composites are promising candidates for a new class of dual electric and magnetic field tunable devices based on ME interactions (Bichurin et al., 2005; Tatarenko et al., 2006). An electric field *E* applied to the composite produces a mechanical deformation in the piezoelectric phase that in turn is coupled to the ferrite, resulting in a shift in the FMR field. The strength of the interactions is measured from the FMR shifts.

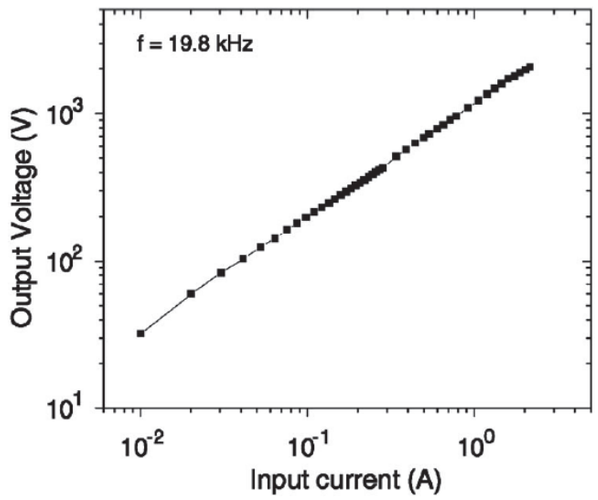

Fig. 12. *I-V* gyration of the ME gyrator.

Ferrite–ferroelectric layered structures enable new paths for making new devices:
(1) Resonance ME effects in ferrite–piezoelectric bilayers, at FMR for the ferrite. The ME coupling was measured from data on FMR shifts in an applied electric field *E*. Low-loss YIG was used for the ferromagnetic phase. Single crystal PMN–PT and PZT were used for the ferroelectric phase; (2) Design, fabrication, and analysis of composite based devices, including resonators and phase shifters. The unique for such devices is the tunability with *E*. Our studies on YIG–PZT composites resulted in the design and characterization of a new class of microwave signal processing devices including resonators, filters, and phase shifters for use at 1–10 GHz. The unique and novel feature in ME microwave devices is the tunability with an electric field. The traditional "*magnetic*" tuning in ferrite devices is

relatively slow and is associated with large power consumption. The "*electrical*" tuning is possible for the composite and is much faster and has practically zero power consumption.

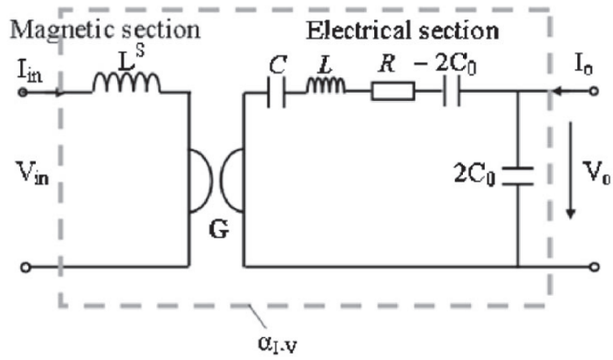

Fig. 13. ME gyration equivalent circuit.

The studies on microwave ME effects in YIG–PZT, YIG–PMNPT, and YIG–BST led to the design, fabrication, and characterization of a new family of novel signal processing devices that are tunable by both magnetic and electric fields. The device studied included YIG–PZT and YIG–BST resonators, filters, and phase shifters. As an example, a stripline ferrite–ferroelectric band-pass filters is considered. Design of our low-frequency ME filter is shown in Fig. 14 and representative data on electric field tuning are shown in Fig. 15. The single-cavity ME filter consists of a dielectric ground plane, input and output microstrips, and an YIG–PZT ME-element. Power is coupled from input to output under FMR in the ME element. A frequency shift of 120 MHz for E = 3 kV/cm corresponds to 2% of the central frequency of the filter and is a factor of 40 higher than the line width for pure YIG. Theoretical FMR profiles based on our model are shown in Fig. 6 for bilayers with YIG, NFO, or LFO and PZT. For E = 300 kV/cm, a shift in the resonance field δH_E that varies from a minimum of 22 Oe for YIG/PZT to a maximum of 330 Oe for NFO–PZT is predicted. The strength of ME interactions $A = \delta H_E / E$ is determined by piezoelectric coupling and magnetostriction.

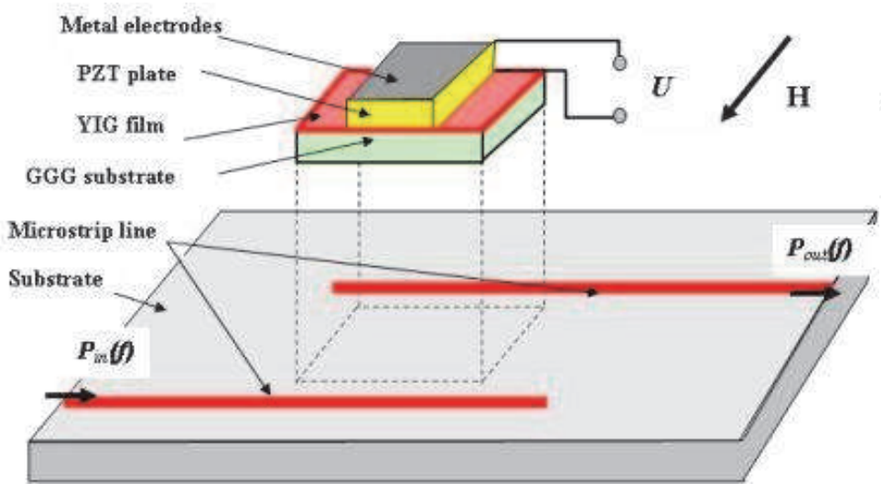

Fig. 14. ME band-pass filter. The ME resonator consisted of a 110 μm thick (111) YIG on GGG bonded to PZT.

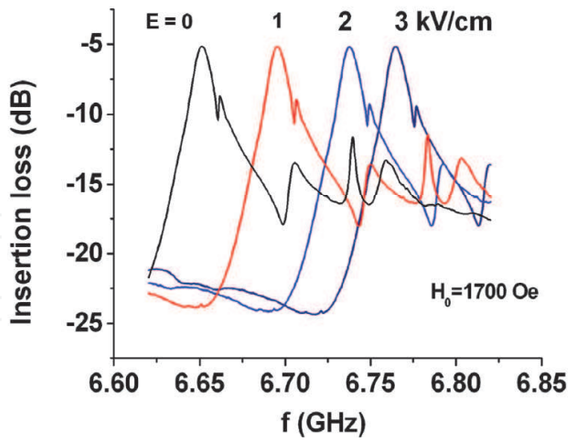

Fig. 15. Loss vs. *f* characteristics for a series of *E* for the YIG–PZT filter.

It is clear from the discussions here that ME interactions are very strong in the microwave region in bound and unbound ferrite–ferroelectric bilayers and that a family of dual electric and magnetic field tunable ferrite–ferroelectric resonators, filters, and phase shifters can be realized. The electric field tunability, in particular, is 0.1% or more of the operating frequency of filters and resonators. A substantial differential-phase shift can also be achieved for nominal electric fields.

9. Conclusions

We discussed detailed mathematical modeling approaches that are used to describe the dynamic behavior of ME coupling in magnetostrictive-piezoelectric multiferroics at low-frequencies and in electromechanical resonance (EMR) region. Our theory predicts an enhancement of ME effect that arises from interaction between elastic modes and the uniform precession spin-wave mode. The peak ME voltage coefficient occurs at the merging point of acoustic resonance and FMR frequencies. The experimental results on lead – free magnetostrictive –piezoelectric composites are presented. These newly developed composites address the important environmental concern of current times, i.e., elimination of the toxic "lead" from the consumer devices. A systematic study is presented towards selection and design of the individual phases for the composite.

There is a critical need for frequency tunable devices such as resonators, phase shifters, delay lines, and filters for next generation applications in the microwave and millimeter wave frequency regions. These needs include conventional radar and signal processing devices as well as pulse based devices for digital radar and other systems applications. For secure systems, in particular, one must be able to switch rapidly between frequencies and to do so with a limited power budget. Traditional tuning methods with a magnetic field are slow and power consumptive. Electric field tuning offers new possibilities to solve both problems.

Ferrite–piezoelectric composites represent a promising new approach to build a new class of fast electric field tunable low power devices based on ME interactions. Unlike the situation when magnetic fields are used for such tuning, the process is fast because there are no inductors, and the power budget is small because the biasing voltages involve minimal

currents. The critical goal for the future is in the development of a wide class of efficient wide band and low-loss electrically tunable magnetic film devices for battlefield radar, signal processing, and secure and experimental evaluation of characteristics. The anticipated advantages of ME devices are yet to be exploited.

10. References

Ahn, C. W., Choi, C. H., Park, H. Y., Nahm, S., Priya, S. (2008)Dielectric and Piezoelectric Properties of (1-x)($Na_{0.5}K_{0.5}$)NbO_3-x$BaTiO_3$ Ceramics, *J. Mat. Sci.* V. 43, (2008), p.p. 6784-6797.

Bichurin, M. I., Petrov V.M., & Fomich, N.N. (1990) *Segnetomagnetic Substances*, Nauka, Moscow. (In Russian).

Bichurin, M.I. (1997) Proceedings of the 3rd International Conference on Magnetoelectric Interaction Phenomena in Crystals (MEIPIC-3, Novgorod, Russia) *Ferroelectrics*, v. 204, (1997), P.p. 1-356.

Bichurin, M.I., Kornev, I. A., Petrov, V. M., Tatarenko, A. S., Kiliba, Yu. V., & Srinivasan, G. (2001) Theory of magnetoelectric effects at microwave frequencies in a piezoelectric-magnetostrictive multilayer composite, *Phys. Rev. B* V. 64, (August 2001) p.p. 094409 (1-6). ISSN 1550-235X

Bichurin, M. I., Petrov, V. M., Kiliba, Yu. V., & Srinivasan, G. (2002) Magnetic and magnetoelectric susceptibilities of a ferroelectricOferromagnetic composite at microwave frequencies, *Phys. Rev*. B. V. 66, (October 2002) p.p. 134404 (1-10).

Bichurin, M. I., Petrov, V. M., & Srinivasan, G. (2003a) Theory of low-frequency magnetoelectric coupling in magnetostrictive-piezoelectric bilayers, *Physical Review B,* V. 68, Issue 5 (August 2003), p.p. 054402 (1-13), ISSN 1550-235X.

Bichurin, M.I., Filippov, D.A., Petrov, V.M., Laletsin, V.M., Paddubnaya N., & Srinivasan, G. (2003b) Resonance magnetoelectric effects in layered magnetostrictive-piezoelectric composites, Phys. Rev.B 68, *Physical Review B,* V. 68, Issue 13 (October 2003), p.p. 132408 (1-4) , ISSN 1550-235X.

Bichurin, M. I., Petrov, V. M., Ryabkov, O. V., Averkin, S. V., & Srinivasan, G. (2005) Theory of magnetoelectric effects at magnetoacoustic resonance in single-crystal ferromagnetic-ferroelectric heterostructures, *Phys. Rev*. B, V. 72, (August 2005), p.p. 060408 (1-4) (R).

Bichurin, M. I., Petrov, V. M., Averkin, S. V.,& Filippov, A. V. (2010) Electromechanical resonance in magnetoelectric layered structures, *Physics of the Solid State* V. 52, Number 10 (October 2010) p.p. 2116-2122. ISSN: 1090-6460

Cai, N., Nan, C. W., Zhai, J. & Lin, Y. (2004) Large high-frequency magnetoelectric response in laminated composites of piezoelectric ceramics, rare-earth iron alloys, and polymers, *Applied Physics Letters*. V. 84, Number 18 (May 2004) p.p. 3516-3518, ISSN 1077-3118.

Chashin, D.V., Fetisov, Y.K., Kamentsev, K.E., & Srinivasan, G. (2008) Resonance magnetoelectric interactions due to bending modes in a nickel-lead zirconate titanate bilayer, *Appl. Phys. Lett.* V. 92, Issue 10 (March 2008), p.p. 102511 (1-3), ISSN 1077-3118.

Cheong, S. W. & Mostovoy, (2007) M. Multiferroics: a magnetic twist for ferroelectricity, *Nature Materials*, Vol. 6, (January 2007). p.p.13-20, ISSN 1476-4660.

Dong, S., Li, J. F., & Viehland, D. (2003). Giant Magneto-Electric Effect in Laminate Composites, *Philosophical Magazine Letters* V. 83, Issue 12 (December 2003) p.p. 769-773, ISSN 1362-3036.

Dong, S., Zhai, J., Bai, F., Li J. F., Viehland, D. (2005) Push-pull mode magnetostrictive/piezoelectric laminate composite with an enhanced magnetoelectric voltage coefficient, *Applied Physics Letters*. V. 87, Issue 6 (August 2005), p.p. 062502 (1-3), ISSN 1077-3118.

Dong, S. X., Zhai, J. Y., Li, J. F., Viehland, D., & Bichurin, M. I. (2006a) Magnetoelectric gyration effect in $Tb_{1-x}Dy_xFe_{2-y}$/Pb(Zr,Ti)O_3 laminated composites at the electromechanical resonance, *Applied Physics Letters*. V. 89, Issue 24 (December 2006) p.p. 243512 (1-3) , ISSN 1077-3118.

Dong, S., Zhai, J., Li, J., & Viehland D. (2006b) Near-ideal magnetoelectricity in high-permeability magnetostrictive/piezofiber laminates with a (2-1) connectivity *Applied Physics Letters*. V. 89, Issue 25 (December 2006), p.p. 252904 (1-3), ISSN 1077-3118.

Fetisov, Y.K., Petrov, V.M., & Srinivasan, G. (2007) Inverse magnetoelectric effects in a ferromagnetic–piezoelectric layered structure, *Journal of Materials Research*. V. 22, Number 8 (August 2007) p.p. 2074-2080. ISSN: 0884-2914

Fiebig, M. (2005). Revival of the magnetoelectric effect. *Journal of physics. D, Applied physics,* Vol. 38, Issue 8 (April 2005) p.p. R123–R152, ISSN 1361-6463.

Filippov, D.A. (2004) Theory of Magnetoelectric Effect in Ferromagnetic–Piezoelectric Bilayer Structures, *Technical Physics Letters,* V. 30, Number 12 (December 2004), p.p. 983-986, ISSN 1090-6533.

Filippov D.A., (2005) Theory of the Magnetoelectric Effect in Ferromagnetic–Piezoelectric Heterostructures, *Physics of the Solid State* V. 47, Number 6 (June 2005), p.p. 1118-1121. ISSN: 1090-6460

Harshe, G., Dougherty, J. O., & Newnham, R. E. (1993) Theoretical Modelling of Multilayer Magnetoelectric Composites. *Int. J.Appl. Electromagn. Mater*. V. 4, (1993), p.p. 145-159.

Huanga, Z. (2006) Theoretical modeling on the magnetization by electric field through product property. *Journal of Applied Physics* V. 100, (2006)p.p. 114104(1-5)

Kimura, M., Ogawa, T., Ando A., & Sakabe, Y. (2002) Piezoelectric properties of metastable (Li,Na)NbO_3 ceramics, *Proceedings of International Conference on Ferroelectrics*, Nara, Japan, 2002.

Kita, E., Takano, S., Tasaki, A., Siratori, K., Kohn, K., & Kimura, S. (1988) Low-temperature phase of yttrium iron garnet (YIG) and its first-order magnetoelectric effect, *Journal of Applied Physics*, Vol. 64, Issue 10 (November 1988), p.p. 5659-5661, ISSN 1089-7550.

Kornev, I., Bichurin, M., Rivera, J.-P., Gentil, S., Jansen, A. G. M., Schmid, H., & Wyder, P. (2000). Magnetoelectric properties of $LiCoPO_4$ and $LiNiPO_4$ *Phys. Rev. B* V. 62, Issue 18 (November 2000) p.p. 12247-12253, ISSN 1550-235X.

Nagata, H. & Takenaka, T. (1991) $(Na_{1/2}Bi_{1/2})TiO_3$ – $BaTiO_3$ System for Lead-Free Piezoelectric Ceramics, *Jpn. J. Appl. Phys.,* V. 30 [9B] (1991) p.p. 2236 – 2239 (1991).

Nan, Ce-Wen, Liu, G., Lin Y., & Chen, H. (2005) Magnetic-Field-Induced Electric Polarization in Multiferroic Nanostructures, Physical Review Letters, V. 94, Issue 19 (May 2005), p.p. 197203 (1-4). ISSN 1079-7114.

Nan, C.-W., Bichurin, M. I., Dong, S., Viehland, D., & Srinivasan, G. (2008), Multiferroic magnetoelectric composites: Historical perspective, status, and future directions, *Journal of Applied Physics*, Vol. 103, (February 2008), p.p. 031101 (1-35), ISSN 1089-7550.

Osaretin, Idahosa A. & Rojas, Roberto G. (2010). Theoretical model for the magnetoelectric effect in magnetostrictive/piezoelectric composites, *Physical Review B,* V. 82, Issue 17 (Novenber 2010), p.p. 174415 (1-8), ISSN 1550-235X.

Petrov, V. M., Srinivasan, G., Bichurin, M. I., & Gupta, A. (2007), Theory of magnetoelectric effects in ferrite piezoelectric nanocomposites, *Phys. Rev. B* V. 75 (June 2007), p.p. 224407 (1-6). ISSN 1550-235X

Petrov, V. M., Srinivasan, G., Bichurin, M. I. & Galkina, T. A. (2009) Theory of magnetoelectric effect for bending modes in magnetostrictive-piezoelectric bilayers, *Journal of Applied Physics* V. 105, Issue 6 (March 2009) p.p. 063911, ISSN 1089-7550.

Prellier, W., Singh, M. P., & Murugavel, P. (2005) The single-phase multiferroic oxides: from bulk to thin film *Journal of Physics: Condensed Matter*. Vol. 17, No. 30, (August 2005), p.p. R803-R832.

Priya, S., Ando A., & Sakabe, Y. (2003a) Nonlead Perovskite materials: $Ba(Li_{1/4}Nb_{3/4})O_3$ and $Ba(Cu_{1/3}Nb_{2/3})O_3$, *J. Appl. Phys*., V. 94 [2] (2003) p.p. 1171 – 1177.

Priya, S., Kim H. W., & Uchino, K. (2003b) Design Consideration for Nonlead Piezoelectric Transformers *Proceedings of International Conference on Intelligent Materials*, State College, USA, 2003.

Ryabkov, O. V., Petrov, V. M., Bichurin, M. I., & Srinivasan, (2006) G. *Tech. Phys. Lett.* V. 32, (2006) p.p. 1021.

Ryu, J., Carazo, A. V., Uchino, K., & Kim, H. (2001). Magnetoelectric Properties in Piezoelectric and Magnetostrictive Laminate Composites, *Japanese Journal of Applied Physics* , V. 40 (May 2001), p.p. 4948-4951, ISSN 1347-4065

Sasaki, A., Chiba, T., Mamiya, Y., & Otsuki, E. (1999)Dielectric and Piezoelectric Properties of $(Na_{1/2}Bi_{1/2})TiO_3$ – $(K_{1/2}Bi_{1/2})TiO_3$ Systems, V. 38 [9B] (1999) p.p. 5564 – 5567.

Srinivasan, G., Rasmussen, E. T., Levin, B. J., & Hayes, R. (2002) Magnetoelectric effects in bilayers and multilayers of magnetostrictive and piezoelectric perovskite oxides. *Physical Review B,* V. 65, Issue 13 (March 2002), p.p. 134402 (1-7), ISSN 1550-235X.

Tatarenko, A.S., Bichurin, M.I., & Srinivasan, G. (2005) Electrically tunable microwave filters based on ferromagnetic resonance in single crystal ferrite-ferroelectric bilayers, *Elec. Lett*., V. 41, (2005), p. 596.

Tatarenko, A.S., Srinivasan, G., & Bichurin, M.I. (2006) A magnetoelectric microwave phase shifter, *Appl. Phys. Lett.,* V. 88, (2006) p.p. 183507 (1-3).

Wang, J., Neaton, J.B., Zheng, H, Nagarajan, V., Ogale, S.B., Liu, B., Viehland, D., Vaithyanathan, V., Schlom, D.G., Waghmare, U.V., Spaldin, N.A., Rabe, K.M., Wuttig, M., & Ramesh, R. (2003) Epitaxial $BiFeO_3$ Multiferroic Thin Film Heterostructures, *Science*, Vol. 299 (March 2003), p.p. 1719-1722, ISSN 1095-9203.

Xing, Z., Dong, S., Zhai, Junyi, Yan, Li, Li, J. & Viehland, D. (2006) Resonant bending mode of Terfenol-D/steel/$Pb(Zr,Ti)O_3$ magnetoelectric laminate composites *Appl. Phys. Lett*. V. 89, Issue 11 (September 2006), pp. 112911 (1-3), ISSN 1077-3118.

Yang, S.-C., Ahn, C.-W., Park, C.-S., & Priya, S. (2011) Synthesis and characterization of lead-free 0.8 $[0.948K_{0.5}Na_{0.5}NbO_3$ – $0.052LiSbO_3]$ – 0.2 $Ni_{0.8}Zn_{0.2}Fe_2O_4$ (KNNLS-NZF)

island - matrix magnetoelectric composites and their application in nickel-based low frequency transducers, *J. Amer. Ceram. Soc.*, (2011) (accepted).

Zhai, J. Y., Li, J. F., Dong, S. X., Viehland, D., & Bichurin, M. I. (2006) A quasi(unidirectional) Tellegen gyrator, J. *Appl. Phys.* V. 100, (2006) p.p. 124509 ISSN 1089-7550.

Zhai, J.,. Xing, Z., Dong, S., Li, J., & Viehland, D. (2008) Thermal noise cancellation in symmetric magnetoelectric bimorph laminates *Appl. Phys. Lett.* V. 93, Issue 7 (August 2008) p.p. 072906 (1-3), ISSN 1077-3118.

Zheng H., Wang J., Mohaddes-Ardabili, L., Wuttig, M., Salamanca-Riba, L., Schlom, D. G., & R. Ramesh, R. (2004) Three-dimensional heteroepitaxy in self-assembled $BaTiO_3$–$CoFe_2O_4$ nanostructures *Applied Physics Letters*. 85, Issue 11 (June 2004), p.p. 2035 (1-3), ISSN 1077-3118.

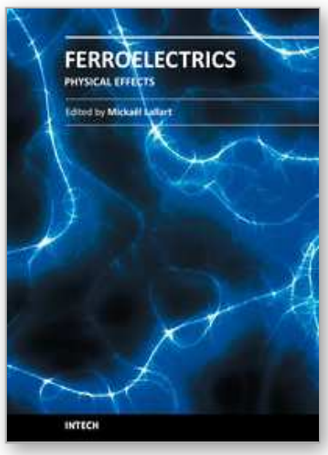

Ferroelectrics - Physical Effects

Edited by Dr. MickaÃ«l Lallart

ISBN 978-953-307-453-5
Hard cover, 654 pages
Publisher InTech
Published online 23, August, 2011
Published in print edition August, 2011

Ferroelectric materials have been and still are widely used in many applications, that have moved from sonar towards breakthrough technologies such as memories or optical devices. This book is a part of a four volume collection (covering material aspects, physical effects, characterization and modeling, and applications) and focuses on the underlying mechanisms of ferroelectric materials, including general ferroelectric effect, piezoelectricity, optical properties, and multiferroic and magnetoelectric devices. The aim of this book is to provide an up-to-date review of recent scientific findings and recent advances in the field of ferroelectric systems, allowing a deep understanding of the physical aspect of ferroelectricity.

InTech Europe
University Campus STeP Ri
Slavka Krautzeka 83/A
51000 Rijeka, Croatia
Phone: +385 (51) 770 447
Fax: +385 (51) 686 166
www.intechopen.com

InTech China
Unit 405, Office Block, Hotel Equatorial Shanghai
No.65, Yan An Road (West), Shanghai, 200040, China
中国上海市延安西路65号上海国际贵都大饭店办公楼405单元
Phone: +86-21-62489820
Fax: +86-21-62489821

IntechOpen